Effects of Sweepback on Unsteady Separation in Mach 5 Compression Ramp Interactions

M. E. Erengil* and D. S. Dolling†
University of Texas at Austin, Austin, Texas 78712

Fluctuating wall pressure measurements have been made upstream of the corner line in Mach 5 compression ramp interactions generated by unswept and 10-, 20-, 25-, 30-, 40-, and 50-deg swept models. The streamwise ramp angle was 28 deg in all cases. The results show the following: 1) In highly swept interactions the rms distributions of pressure fluctuations as well as the mean distributions are essentially quasiconically symmetric. The rms levels decrease globally with increasing sweep as does the maximum rms generated by the translating separation shock. 2) The length of the intermittent region, over which the separation shock foot translates, decreases with increasing sweep. In a given interaction, the length of the intermittent region grows spanwise. 3) Dominant separation shock frequencies increase from about 0.3–0.5 kHz in unswept flows to about 2–7 kHz in highly swept flows. In a given interaction, shock frequencies decrease spanwise. 4) The higher frequencies are shown to be a direct result of the decrease in the length scale of the separation shock motion.

Introduction

THE unsteadiness of shock wave/turbulent boundary-layer interactions (SWTBLI) has become an increasingly active area in high-speed aerodynamics research. This unsteadiness generates large-amplitude fluctuating pressure loads that unfortunately also usually occur in regions of high heating rates. Fluctuating pressure loads and high heating rates can lead to poor aerodynamic performance and early fatigue of structures. It is therefore important that the locations of these loads as well as their severity be known at the design stage. Thus, detailed quantitative data on the unsteadiness of these interactions are needed to understand the flow-field physics better and to develop correlations useful for engineering design.

Although experimental evidence from as early as the 1950s has shown that the boundary-layer separation and reattachment processes in SWTBLI can be unsteady,[1] the phenomenon has only been studied extensively in the last decade. Most of the investigations have focused on nominally two-dimensional problems, such as interactions generated by unswept compression corners,[2-4] or the flowfield along the line of symmetry upstream of the leading edge in three-dimensional interactions generated by cylinders,[5] or blunt fins.[6] These studies have shown that the unsteadiness is characterized by large-amplitude, low-frequency pressure fluctuations generated by the separation shock foot in random motion. More recent investigations of such flows focused on the dynamics of the separation and reattachment processes,[7] the structure of the separation shock system,[8] and the spanwise rippling motion of the separation shock.[9] In brief, it has been shown that the flow immediately downstream of the instantaneous location of the separation shock foot is separated. Hence, the intermittent region (i.e., the region in which the separation shock foot translates) is, in fact, a region of intermittent separation. The dominant motion of the separation and reattachment locations is best described as expansion and contraction of the separation bubble. Similar results have been reported by Kus-

soy et al.[10] in a Mach 3 interaction generated by a tilted 30-deg half-angle cone attached to a circular cylinder.

In contrast, relatively little is known about the unsteadiness of separation in swept interactions because most of the investigations of such flows have focused on the mean properties. Such techniques as surface flow visualization have been used extensively in sharp fin and compression ramp flows to study the evolution of the interaction footprint as the flow is progressively swept. A recent review of such flows can be found in Ref. 11. In swept compression ramp interactions, which have been studied quite extensively, mean measurements have shown that two flow regimes, cylindrical and quasiconical, exist.[12] In cylindrically symmetric interactions, the upstream influence line UI, the separation line S, and the corner line C are parallel to each other, whereas in quasiconical interactions these lines belong to a family of rays that emanate from a common point called the virtual conical origin (VCO). In both cases, there is an inception zone between the ramp apex and the region in which symmetry is reached. For a given streamwise ramp angle α the interaction footprint is cylindrically symmetric for moderately swept flows and becomes quasiconical as the sweepback angle λ_C is increased.

To the authors' knowledge Tran,[13] Tan et al.,[14] and Tran et al.[15] were the first to study the unsteadiness of swept interactions using sharp fins at angle of attack in Mach 3 flow in the mid-1980s. In addition, Tran[13] made limited measurements in highly swept interactions generated by a 24-deg compression corner with sweepback angle of 60 deg and a semicone with half-angle of 25 deg. The measurements revealed large-amplitude, low-frequency pressure fluctuations attributable to an unsteady separation shock foot. Schmisseur and Dolling[16] have also studied sharp fin-induced interactions in Mach 5 flow, at higher angles of attack and in a thicker boundary layer. Their results also showed the emergence of pressure fluctuations characteristic of the unsteady separation shock as the fin angle of attack is increased.

Recently, Dolling et al.[17] completed the first phase of a systematic investigation at Mach 5 in which the effects of sweepback on the separation shock dynamics in compression ramp interactions is being examined. Detailed measurements of surface pressure fluctuations were made near the separation line S at three different spanwise positions in interactions generated by 28-deg compression ramp models with sweepback angles λ_C of 10 and 20 deg, respectively. Their results showed that the separation shock dynamics and local flow structure were qualitatively similar to those in unswept interactions. Quantitatively, however, the results showed a

*Graduate Student, Department of Aerospace Engineering and Engineering Mechanics. Student Member AIAA.
†Professor, Department of Aerospace Engineering and Engineering Mechanics. Associate Fellow AIAA.

decrease in intermittent region length scale and maximum rms and an increase in separation shock frequencies.

The current study is the second phase of this systematic investigation, in which four additional models with constant streamwise angles of 28 deg and sweepback angles of 25, 30, 40, and 50 deg have been used. Results from both studies have been compiled and presented in this paper. The objectives of this study are twofold: 1) to determine qualitatively and quantitatively the effects of sweepback on the dynamics of unsteady separation in compression ramp interactions and 2) to determine the variations, if any, in the dynamics of unsteady separation in the spanwise direction.

The results presented in this paper document the effects of sweepback on unsteady separation in compression ramp interactions. Additional questions regarding the cause(s) of separation shock unsteadiness and variations in intermittent length scales with sweepback are being addressed in an ongoing study. These results will be reported in a later paper.

Experimental Program

Wind Tunnel and Flow Conditions

Experiments were conducted in the high Reynolds number, Mach 5 blowdown wind tunnel at the Balcones Research Center of the University of Texas at Austin. The rectangular test section of this tunnel is 15.24 cm (6 in.) wide, 17.78 cm (7 in.) high, and 30.48 cm (12 in.) long. Up to 3.964 m^3 (140 ft^3) of compressed air stored at about 17.24 MPa (2500 psia) provides run times of up to 1 min for the current stagnation conditions. Two banks of 420 kW nichrome wire resistive heaters are used to heat the incoming air and can provide stagnation temperatures of up to 422 K (759°R) in the settling chamber.

All tests were conducted at a stagnation pressure of 2.28 MPa (330 psia) and a stagnation temperature of 359 K (647°R), which generate a freestream unit Reynolds number of 49.9×10^6 m^{-1} (15.2×10^6 ft^{-1}). The freestream Mach number and velocity in the test section were 4.95 and 775 m/s (2543 ft/s), respectively. The incoming turbulent boundary layer underwent natural transition and developed under approximately adiabatic wall temperature conditions. Boundary-layer parameters were determined from pitot surveys made with a probe having a tip orifice 0.020 cm (0.008 in.) high and 0.038 cm (0.015 in.) wide. Total temperature surveys were also made. In the data reduction, the static pressure through the boundary layer was assumed constant and equal to the freestream value. A good fit to law of the wall/law of the wake was obtained for the mean velocity profile. Boundary-layer parameters measured at 94.47 cm (37.98 in.) downstream of the throat on the tunnel centerline are listed in Table 1.[18]

Models and Instrumentation Plug

Four swept and one unswept compression ramp models were tested. The unswept 28-deg model was made of aluminum and was 12.7 cm (5 in.) wide and 3.8 cm (1.5 in.) high. All four of the swept models, made of brass, had a constant streamwise angle α of 28 deg and sweepback angles λ_C of 25, 30, 40, and 50 deg. They were 10.8 cm (4.25 in.) wide and 5.1 cm (2 in.) high. Two aluminum aerodynamic fences with sharpened leading edges were attached to the sides of the unswept ramp to prevent spillage and isolate the interaction from the sidewall boundary layers. Only one stainless steel aerodynamic fence with a sharpened leading edge was attached to the apex side of the swept models to prevent spillage and isolate the interaction from the sidewall boundary layer. The fence leading edge extended at least 6.4 cm (2.5 in.) ($\approx 4\delta_o$) upstream of the apex. All models were mounted on the tunnel floor and could be moved in the streamwise direction with infinite resolution. A sketch of the experimental arrangement and a swept compression ramp model, instrumentation plug, and the coordinate system are shown in Fig. 1.

The transducers could be mounted flush along four different rows in an 8.57 cm (3.375 in.) diam brass plug centered

Table 1 Boundary layer parameters

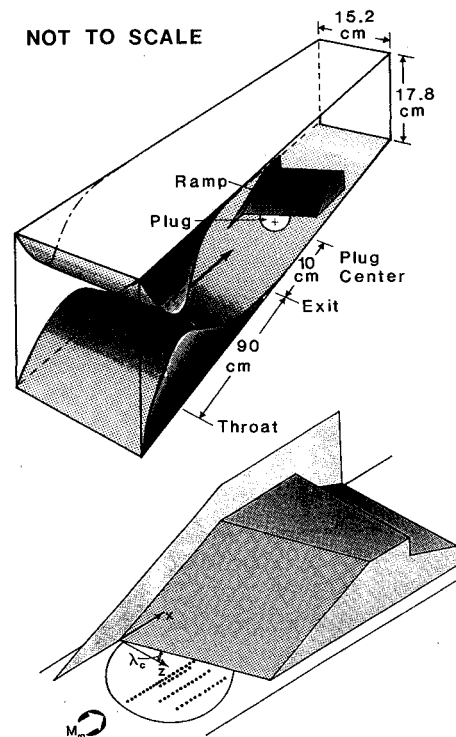| Parameter	
δ_o, cm (in.)	1.51 (0.59)
δ^*, cm (in.)	0.67 (0.26)
θ ($\times 10^2$), cm (in.)	6.61 (2.60)
Π	0.78
$H \equiv \delta^*/\theta$	10.20
Re_θ ($\times 10^{-4}$)	3.16
C_f ($\times 10^4$)	7.74

Fig. 1 Isometric sketch of experimental arrangement, model, and transducer plug.

97.00 cm (38.19 in.) downstream of the nozzle throat. The four rows of transducer ports could be aligned at any angle to the freestream. The first row is along the plug centerline and has 26 transducer ports. The second (8 ports), third (13 ports), and fourth (12 ports) rows are parallel to the center row and are spaced 0.29 cm (0.115 in.), 1.27 cm (0.500 in.), and 2.54 cm (1.000 in.) from the latter, respectively (see Fig. 1). An additional row of transducer ports was also machined in the tunnel floor to allow measurements farther outboard. This row has nine transducer ports and it is at a fixed angle of 30 deg to the undisturbed freestream. In any given row, the spacing between two adjacent ports ζ is 0.29 cm (0.115 in.). Customized dummy brass plugs were mounted flush in the unused transducer ports.

Instrumentation and Data Acquisition System

Up to eight miniature, Kulite, high-frequency response pressure transducers were used. These were either XCW-062-15A, 0–103 kPa (0–15 psia), or XCQ-062-50A, 0–345 kPa (0–50 psia), absolute pressure transducers, and all had outer diameters of 0.159 cm (0.0625 in.) and 0.071 cm (0.028 in.) diam pressure-sensitive diaphragms. As quoted by the manufacturer, the natural frequency response of the diaphragm was 250 kHz (for 0–103 kPa models) and 500 kHz (for 0–345 kPa models). However, perforated screens protecting the transducers from dust particles limit the effective frequency response of both types of transducers to about 50 kHz. All transducers

were calibrated statically using a Heise digital pressure gauge (Model 710A) accurate to within 6.9 Pa (0.001 psia).

Output from the pressure transducers was first amplified by either Dynamics (Model 7525), Measurements Group (Model 2311), or PARC (Model 113) amplifiers, and then low-pass filtered using Ithaco (Model 4113 or Model 4213) analog filters. Amplifier gains were adjusted for maximum resolution and varied depending on the transducer type and the position of the transducer in the interaction. Filter cutoff frequencies were set at 50 kHz for sampling rates of 100 kHz or more and were reduced to at most one-half of the sampling frequency for tests in which the sampling rates were lower than 100 kHz.

Filtered signals were then digitized by two LeCroy Model 6810 Waveform Recorders equipped with 12-bit analog-to-digital (A/D) converters, each of which had two Megawords of memory, and could sample up to 4 channels of data simultaneously, at rates up to 1 MHz per channel. Both A/D converters were triggered using the same clock, thus 8 channels could be sampled simultaneously at rates up to 1 MHz per channel. A maximum of 4096 records (1 record = 1024 datapoints) of data could be obtained. Further, each channel could be adjusted individually allowing the user to optimize each channel for different input signal ranges.

Data were then downloaded to an HP 9000 Model 370 minicomputer and stored on tape for later analysis. All analyses were performed either on the primary computer (Model 370) or on one of the two HP 9000 Model 340 workstations connected to the primary computer.

Test Program

In high-speed flows, surface tracer techniques, such as the kerosene-lampblack-diesel method, are widely used to locate separation lines. In this case, the mixture is painted on the tunnel floor and compression ramp face before tunnel startup, and after shutdown the pattern is lifted off the surface on large sheets of transparent tape. Because the mixture responds to surface shear stress τ_w, the surface flow directions and hence features such as the separation and attachment lines can easily be deduced. These surface patterns were used to align the transducer rows at the desired orientation. However, this method has essentially zero frequency response, and the resulting pattern is that generated by the mean wall shear stress field.

Fluctuating wall pressure measurements were made perpendicular to the local separation line along three different spanwise rows. Two runs were made along each row. In the second run, the model was moved by about one-half of the minimum transducer spacing in the streamwise direction to improve the spatial resolution. It should be noted that the motion of the ramp changes the spanwise location of the row slightly. However, the change is negligible. Two additional runs were made to acquire data from the transducers in the tunnel floor for the 30-, 40-,and 50-deg swept interactions. To investigate the spanwise evolution of the pressure fluctuations, measurements were also made along the corner line at the compression ramp test surface junction. Measurements were also made along spanwise lines immediately upstream of the separation line in 30-, 40-, and 50-deg swept interactions.

Almost all data were sampled at 200 kHz/channel and filtered at 50 kHz. To improve the frequency resolution, some experiments were repeated and sampled at 50 kHz, in which case the filter cutoff frequency was set at 25 kHz. Typically 250 records (1 record = 1024 datapoints) of data were taken per channel. The earlier data obtained in moderately swept interactions by Boitnott[19] were also reanalyzed and some of the results will be presented in this paper. Available data thus span a wide range of sweepback angles (0, 10, 20, 25, 30, 40, and 50 deg).

Analysis Techniques

Standard time-series analyses and conditional sampling algorithms have been used to analyze the data. A detailed de-

scription of the conditional sampling algorithm, the two-threshold-method boxcar conversion technique, can be found in Ref. 6. For completeness, a very brief description follows. In addition, a new analysis technique using boxcar functions is described in some detail.

Boxcar Conversion Technique

This technique is applied to signals measured under the unsteady separation shock and extracts shock passages from the pressure fluctuations using a two-threshold method. The thresholds are set at $T_1 = \bar{P}_{wo} + 3\sigma_{P_{wo}}$ and $T_2 = \bar{P}_{wo} + 6\sigma_{P_{wo}}$, where $\bar{P}_{wo}$ is the undisturbed turbulent boundary-layer mean pressure level and $\sigma_{P_{wo}}$ is the rms of the turbulent boundary-layer pressure fluctuations. These threshold settings were recommended following a sensitivity analysis of the effects of T_1 and T_2 (Ref. 6). A similar sensitivity analysis showed that the same threshold settings were appropriate for the analysis of data from swept flows. In the two-threshold method, the boxcar is generated when $P_w(t) > T_2$ and is terminated when $P_w(t) < T_1$. Thus, when the boxcar assumes a value of 1, this signifies a shock passage in the upstream direction and is called the risetime. Similarly, when it assumes a value of 0, this signifies a shock passage in the downstream direction, and is called the falltime. Once a shock passage is detected using T_1 and T_2 and an initial fall-time assigned, a counter is then used to march backward in time until the instantaneous value $P_w(t)$ is found, which is just below T_2. The falltime is then reassigned to this new value. The requirement that the rise and falltimes be determined by the same threshold level, (i.e., T_2), ensures that the separation shock foot is at the same position at both rise- and fall-times. Further, these times are the only pertinent information in the generation of the separation shock foot history, which is explained in some detail in the following section.

Separation Shock Foot Position History

Separation shock dynamics have so far been deduced and interpreted from surface pressure fluctuations because to date there have been no direct measurements of separation shock foot histories $X_s(t)$ in interactive flows of this type. Naturally, it would be preferable to discuss and compare separation shock dynamics literally, i.e., in terms of $X_s(t)$. Even though it is necessarily approximate, simultaneous measurements of multichannel pressure fluctuations coupled with conditional algorithms allow $X_s(t)$ to be deduced in a piecewise continuous form. This technique provides a means through which the separation shock dynamics in one interaction can be compared directly with the shock dynamics in a different interaction.

Separation shock foot position history is generated from nested boxcar sequences such as those shown in Fig. 2, which are deduced from simultaneous measurements of surface pressure fluctuations made in the intermittent region. The example shown is for the unswept interaction. The schematic in Fig. 2a shows the position of transducers upstream of the separation line and the corresponding bin numbers. Nested boxcar functions from actual data are shown for channels 2 through 6 in Fig. 2b. The rise and falltimes in the nested boxcar sequence and the channel on which they occur define the time and position coordinates of the separation shock foot, respectively. Linear interpolation of these coordinates yields a piecewise smooth function for $X_s(t)$ as depicted in Fig. 2c. In this conversion, the only assumptions are that the shock moves in a unidirectional motion and at a constant speed from one bin to the other. In the case of a shock turnaround, it is further assumed that the shock moves to the middle of the bin, changes its direction of motion, and moves back at the same speed. It should be noted that these assumptions are not new and have always been implicit in conditional analysis techniques employed previously. Furthermore, the separation shock velocity $V_s(t)$ can be calculated by taking the derivative of $X_s(t)$. The authors are aware of the problems involved in
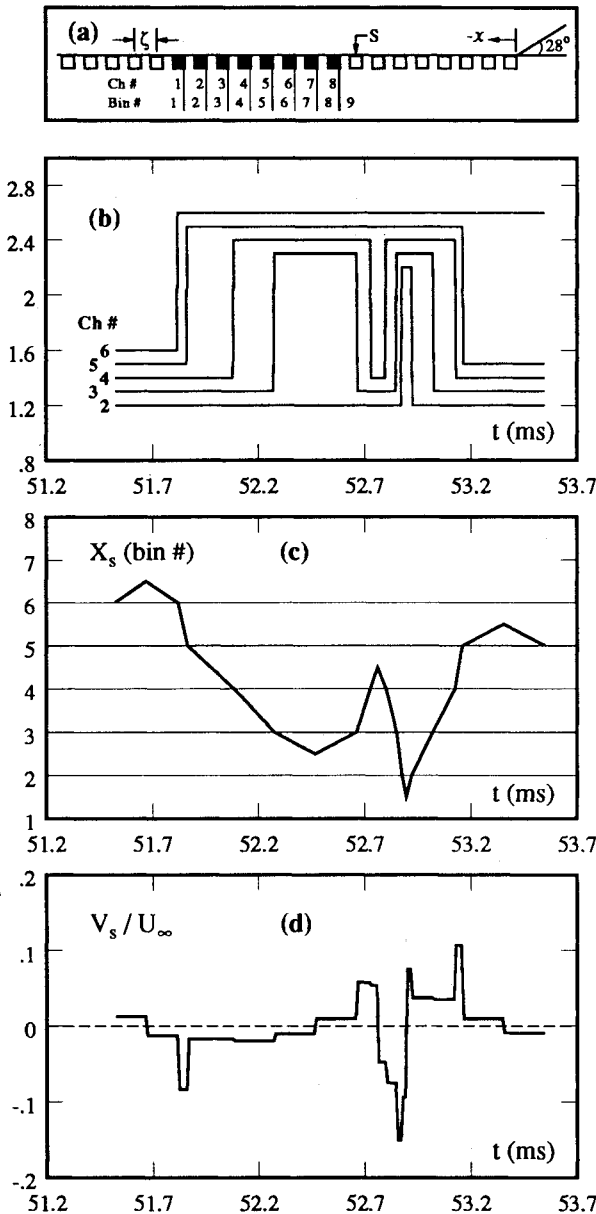
Fig. 2 Conversion technique for separation shock foot position history.

also analyzed. Results from all swept interactions as well as those from the unswept interaction are presented below. It should be noted that all pressure results are normalized by the incoming undisturbed mean boundary-layer pressure $\bar{P}_{wo}$, which is assumed to be equal to the freestream pressure of 4.56 kPa (0.661 psia).

Surface Flow Patterns

Surface flow patterns are shown in Figs. 3a–3f for sweepback angles λ_C of 10, 20, 25, 30, 40, and 50 deg, respectively. The apex side of each model is indicated by a solid line and the compression corner is delineated by a black and white line. Separation lines, corner lines, and attachment lines are indicated by S, C, and A, respectively. To provide a measure of the physical scale, the incoming boundary layer thickness δ_0 is also shown in each figure.

Clearly, the 10-deg case is cylindrically symmetric. However, the portion of the 20-deg interaction captured by the flow visualization appears to be in the inception zone, and based on the arguments of Dolling et al.,[17] it will probably develop cylindrically. As the flow is swept back from 20 to 25 deg, the separation region length scale upstream of the corner decreases noticeably. For $\lambda_C \geq 25$ deg, the interactions all appear to be quasiconical, based on their surface flow patterns. The location of the VCO was determined by finding the intersection point of straight lines drawn through the separation line S, the corner line C, and the attachment line A. The distance to the VCO, R_{VCO}, which is given in Table 2, is the radial distance from the apex of the model. The sweepback angle of the separation line λ_s and that of the attachment line λ_A are also given in Table 2 along with the radial distances to the end of the inception zone R_{IZ} and each of the transducer rows R_M, R_{O1}, R_{O2}, and R_F. The subscripts M, $O1$, $O2$, and

differentiating the experimental data. However, in this case $V_s(t)$ can only be calculated by dividing the distance between two adjacent transducers by the time it takes for the shock to cross both transducers. Note that this is equivalent to differentiating $X_s(t)$. The corresponding velocity history normalized by U_∞ is shown in Fig. 2d.

Once the conversion to $X_s(t)$ is completed, the raw data for calculating the separation shock dynamics are defined for that particular interaction and can be analyzed using standard time-series analysis techniques and compared directly with the separation shock dynamics from a different interaction.

Discussion of Results

To recap, surface pressure fluctuations have been measured near separation lines in interactions generated by swept compression ramp models with constant streamwise angle $\alpha = 28$ deg and sweepback angles $\lambda_C = 25$, 30, 40, and 50 deg. Measurements were made along three spanwise rows aligned perpendicular to the local separation line. Similar measurements made by Boitnott[19] using 28-deg compression ramp models with moderate sweepback angles of 10 and 20 deg were
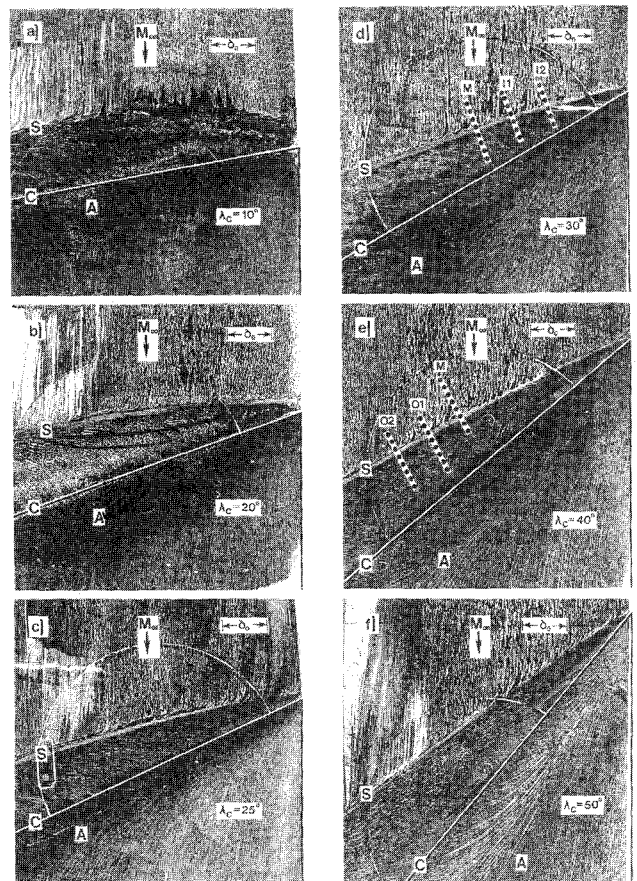

Fig. 3 Surface flow patterns ($10 \leq \lambda_C \leq 50$ deg) for swept compression ramp interactions.

Table 2 Mean flow features and locations of the transducer rows

λ_C:	25 deg	30 deg	40 deg	50 deg
λ_S	16.0	19.5	28.5	36.5
λ_A	30.0	37.0	49.0	65.0
R_{VCO}, cm (in.)	4.19 (1.65)	2.72 (1.07)	2.08 (0.82)	1.07 (0.42)
R_{IZ}, cm (in.)	9.27 (3.65)	6.22 (2.45)	5.08 (2.00)	3.20 (1.26)
R_M, cm (in.)	9.14 (3.60)	7.80 (3.07)	7.62 (3.00)	7.01 (2.76)
R_{O1}, cm (in.)	10.41 (4.10)	9.07 (3.57)	8.89 (3.50)	8.28 (3.26)
R_{O2}, cm (in.)	11.68 (4.60)	10.34 (4.07)	10.16 (4.00)	9.55 (3.76)
R_F cm (in.)		12.24 (4.82)	12.32 (4.85)	12.52 (4.93)
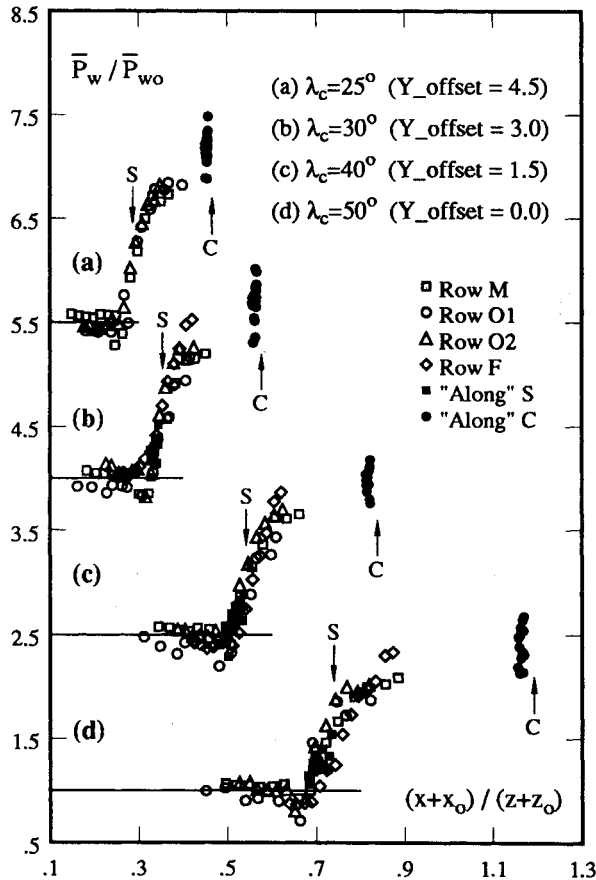
Fig. 4 Distributions of $\bar{P}_w/\bar{P}_{wo}$ in conical coordinates.

F correspond to the middle row, two outer rows, and the tunnel floor row, respectively. Note that all but the tunnel floor row F are shown in Fig. 3e.

Mean and Standard Deviation Distributions

Distributions of normalized mean wall pressure $\bar{P}_w/\bar{P}_{wo}$ are plotted in conical coordinates $(x + x_o)/(z + z_o)$, in Figs. 4a–4d for $\lambda_C = 25$, 30, 40, and 50 deg, respectively. In this coordinate system, $(x + x_o)/(z + z_o)$ is the tangent of the sweepback angle of a conical ray emanating from the VCO. Thus, x_o and z_o are the streamwise and spanwise components of R_{VCO} which is given in Table 2. The separation and corner lines are indicated by S and C in all figures. The scatter in the data in Figs. 4a–4d is indicative of the difficulties involved in measuring such low pressures using 0–345 kPa (0–50 psia) transducers. Nevertheless, the general trends are captured and agree with results from earlier investigations.[20] $\bar{P}_w$ increases from the undisturbed boundary-layer pressure and asymptotes towards a plateau level in the separated region upstream of the corner. Also evident in these figures is the extremely rapid rise in $\bar{P}_w$ immediately upstream of the corner, which agrees with earlier experimental results at Mach 3.[20] These data are gener-

ated from measurements made along the corner line as indicated in the legend in Fig. 4.

Distributions of normalized standard deviation $\sigma_{Pw}/\bar{P}_{wo}$ are plotted in conical coordinates, $(x + x_o)/(z + z_o)$ in Figs. 5a–5d for $\lambda_C = 25$, 30, 40, and 50 deg, respectively. Again, separation and corner lines are indicated by S and C in all figures. The good collapse of data, particularly in the region of rapid rise upstream of S, shows quite clearly that the rms distributions are also quasiconically symmetric. The scatter in maximum rms in the vicinity of S is probably due to spatial resolution problems, because the diameter of the transducer is, in some cases, comparable to the distance over which the rise to the maximum rms occurs. The intermittent region grows quasiconically, and thus the maximum rms levels are higher along the outer rows because the spatial resolution is better. Even though the absolute values of the maximum rms may be underestimated along the inner rows, the trends with increasing sweepback are certainly quite clear, and meaningful comparisons can be made.

The results in Fig. 5 show that the normalized rms levels throughout the interaction upstream of the corner decrease with increasing sweep. Furthermore, the rms peak in the intermittent region, which is indicative of a translating separation shock foot, decreases. This decrease suggests that the intensity of the unsteadiness diminishes with increasing sweep. An interesting feature in the rms distributions (as in the mean distributions) is the presence of very steep gradients immediately upstream of the corner. There may be a second, and perhaps a larger, peak in rms along the corner line than in the intermittent region. However, the physical cause cannot be resolved with available data. More measurements with much better spatial resolution are required both upstream and downstream of the corner line.

To examine this issue further, the normalized rms values along the corner line are plotted vs the normalized radial
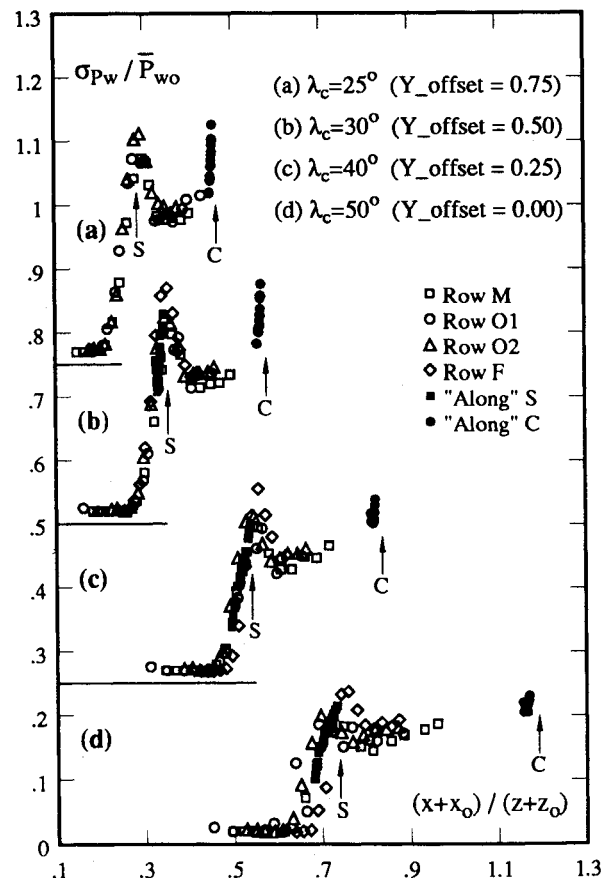
Fig. 5 Distributions of $\sigma_{Pw}/\bar{P}_{wo}$ in conical coordinates.

distance r/δ_o in Fig. 6. Almost all measurements were made in regions of quasiconical symmetry, and yet the rms values immediately upstream of the corner line increase radially. Even though the transducers were aligned along the corner line, with increasing radial distance the center of each consecutive transducer falls on a different ray progressively approaching the ray that passes through the corner. Normally, such small variations would not be important but in this region the gradients are very steep and very small angular changes result in large changes in both $\bar{P}_w$ and σ_{Pw}. It appears that, with the exception of the 25-deg interaction, the rms values immediately upstream of the corner line decrease with increasing sweepback.

Variation of Maximum Standard Deviation with Sweepback

The normalized maximum standard deviation $(\sigma_{Pw})_{max}/\bar{P}_w$ in the intermittent region from each row is plotted vs the local sweepback angle of the separation line λ_S in Fig. 7. It should be noted that λ_S was chosen for convenience, and that the authors do not intend to suggest that maximum rms is solely a function of the local sweepback angle of the separation line. Nevertheless, results clearly show that maximum standard deviation decreases with increasing λ_S; the decrease is more than a factor of 2 as the separation line is swept back from 0 to 36.5 deg. Again, small differences in the maximum rms levels at the same λ_S in highly swept interactions are probably due to spatial resolution problems as discussed earlier.

Wall Pressure Signal Characteristics

Before the effects of sweepback on the unsteady separation are discussed in more detail, it is probably useful to describe qualitatively the changes in wall pressure fluctuations that occur because it is from them that the separation shock dynamics are deduced. Figures 8a-8c show typical fluctuating pressure signals and their corresponding amplitude probability density functions (PDFs) measured upstream of the separation line in unswept, 20-, and 40-deg swept interactions, respectively. Pressure signals from the unswept and moderately swept ($\lambda_C = 20$ deg) interactions are qualitatively similar in that they both have high-amplitude, low-frequency pressure fluctuations superimposed on the low-amplitude, high-frequency pressure fluctuations characteristic of the undisturbed turbulent boundary layer. Two distinct pressure levels, i.e.,
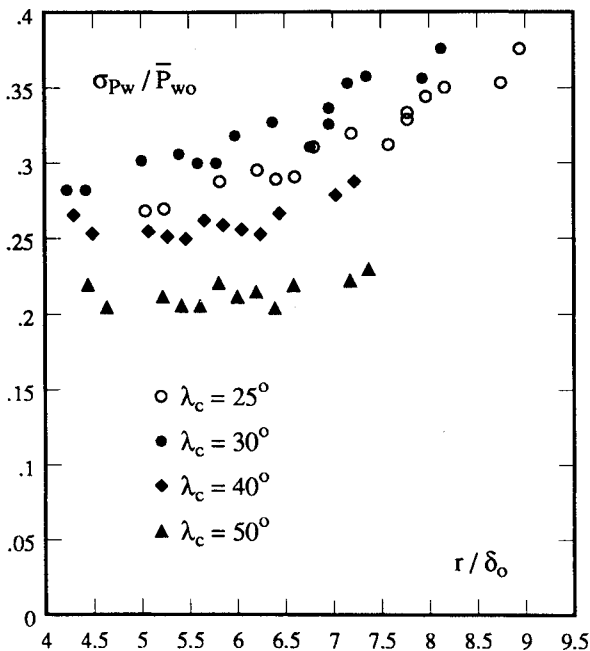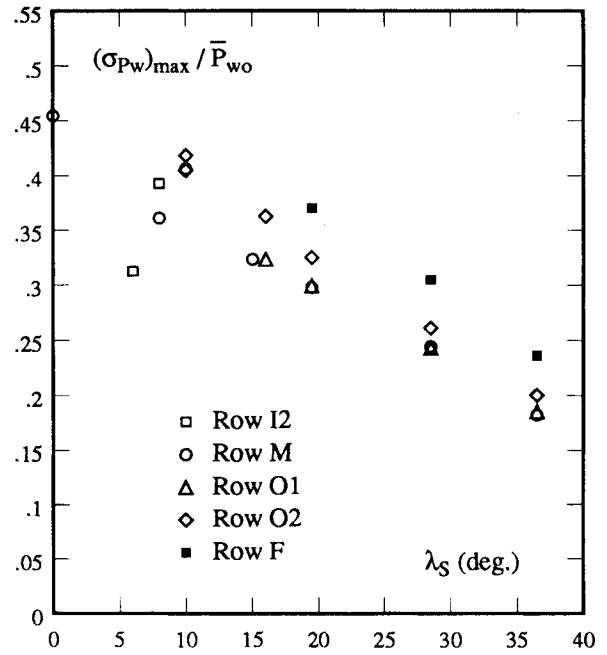

Fig. 7 Variation of $(\sigma_{Pw})_{max}/\bar{P}_{wo}$ with local sweepback angle of the separation line λ_S.

that of the undisturbed turbulent boundary layer and a higher level downstream of the separation shock/compression system, are clearly evident either through visual inspection of the pressure histories or from the corresponding bimodal PDFs. The pressure signal from the highly swept interaction ($\lambda_C = 40$ deg), on the other hand, is quite different: the secondary peak in the corresponding PDF is no longer present. Furthermore, the signal in Fig. 8c has lower amplitude fluctuations at much higher frequencies. However, it should be noted that this signal is also intermittent and that it can be analyzed using the two-threshold-method conditional sampling techniques.

In brief, the amplitude of the wall pressure fluctuations decreases while their frequencies increase with increasing sweep. This change is gradual with increasing sweep for small sweepback angles ($\lambda_C = 20$ deg), but becomes more rapid as the sweepback increases ($\lambda_C = 25$ deg).

Power Spectra in the Intermittent Region

Signals sampled at 200 kHz were used to calculate the power spectra in the unswept and 25-, 30-, 40-, and 50-deg swept interactions. At this sampling rate the frequency resolution is about 195 Hz. Those data from Ref. 19 (i.e., $\lambda_C = 10$ and 20 deg) were sampled at 110 kHz resulting in a frequency resolution of about 107 Hz. For a fixed λ_C, the frequency content of pressure signals near the separation line was independent of position in the intermittent region along a given row. For this reason, only those power spectra at maximum rms are shown in the normalized form in Fig. 9 for row $O2$. Results from all seven interactions are plotted and identified in the legend.

Dominant frequencies, which in this region are due to the separation shock motion, increase from about 0.3-0.5 kHz in the unswept interaction to about 2-7 kHz in the 50-deg swept interaction. This increase in dominant frequencies is initially small as the interaction is swept from $\lambda_C = 0$ to 20 deg but becomes more rapid with increasing sweep ($\lambda_C = 25$ deg). Because the dominant pressure fluctuations are a result of the separation shock motion, these figures clearly demonstrate that the separation shock crossings occur at much higher frequencies in swept interactions than they do in the unswept case, for a fixed incoming turbulent boundary layer. Separation shock dynamics per se will be discussed in more detail in the following sections.
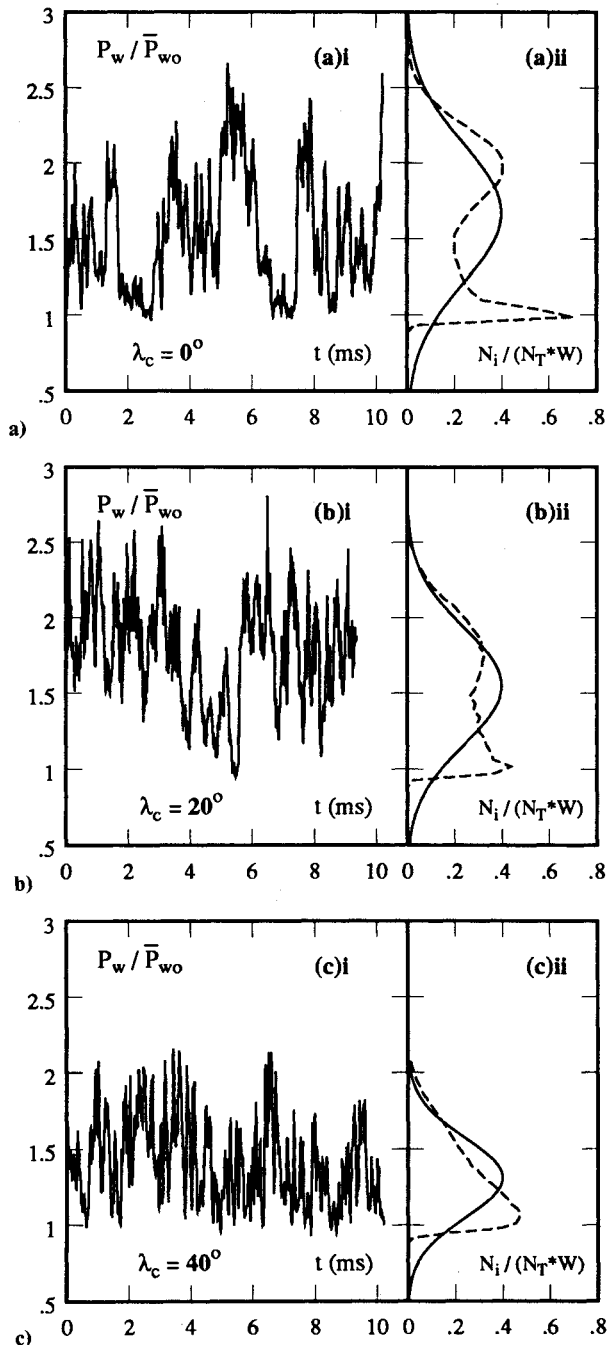

Fig. 6 Variation of $\sigma_{Pw}/\bar{P}_{wo}$ along corner line.

Fig. 8   Typical wall pressure histories and corresponding probability density functions for $\lambda_C = 0$, 20, and 40 deg.

Intermittent Region Length

All results presented so far have been obtained using standard time-series analysis techniques. Questions regarding the separation shock dynamics, however, can best be addressed using conditional sampling algorithms, some of which have been discussed in the Analysis Techniques section of this paper. Most of the following results discussed below have been obtained using such algorithms.

The intermittent region is the region in which the separation shock foot translates. Intermittency γ at a point in the intermittent region is the fraction of total time that the separation shock foot is upstream of that point. Whether it is upstream or downstream has been determined using the two-threshold boxcar conversion technique developed by Dolling and Brusniak[6] and was briefly explained earlier. By definition, the intermittent region length L_i extends from $\gamma \approx 0.0$ to 1.0 and is determined from the intermittency distribution. In the un-

swept interaction, measurement of the intermittency distribution is a fairly straightforward task. In swept interactions, however, there are two complicating factors. First is the spatial resolution problem, which arises due to the shrinking of the intermittent region. Second, the evolution of the surface pressure fluctuations with sweep is such that there is a blurring of the distinction between disturbed and undisturbed levels in the pressure histories. This blurring is directly attributable to the fact that the shock motion is at higher frequency and occurs over a shorter distance. These two factors in combination make it difficult to calculate the intermittency at stations that have large values. The net result is that the downstream end of the intermittent region is undetectable directly. In fact, the maximum detectable intermittency decreases as the interaction is progressively swept back. The distance from $\gamma \approx 0.02$ to 0.98 is taken as the length of the intermittent region. For those cases, in which the downstream end of the intermittent region could not be detected, the distance from $\gamma \approx 0.02$ to 0.50 was measured and then doubled. This procedure is justified since the separation shock foot position within the intermittent region is randomly distributed (as will be shown later).

Figure 10a shows the normalized length of the intermittent region L_i/δ_o as a horizontal line for the unswept and the moderately swept interactions ($\lambda_C \leq 20$ deg). Since highly swept interactions ($\lambda_C \geq 25$ deg) are quasiconically symmetric, it is more appropriate to define the intermittent region length in terms of an angular increment rather than in terms of δ_o. Figure 10b shows the angular extent of the intermittent region by a vertical line drawn from λ_0 to λ_1. Here, λ_0 and λ_1 are the sweepback angles of rays along which the intermittency is about 0.02 and about 0.98, respectively. In this representation, each line forms a scale ranging from $\gamma \approx 0.98$ to 0.02. The relative position of the separation line from the flow visualization is also indicated on each of these lines. The decreasing length of the horizontal lines (and the vertical ones in highly swept interactions) shows quite clearly the shrinking of the intermittent region as the interaction is progressively swept back. Furthermore, the changing position of the marker indicating the location of the separation line shows that the separation location from surface flow visualization moves upstream in the ¦ ·termittent region toward lower and lower values of inter.ᵢₙ.tency. A plausible explanation of why this forward motion of the separation line occurs was given by
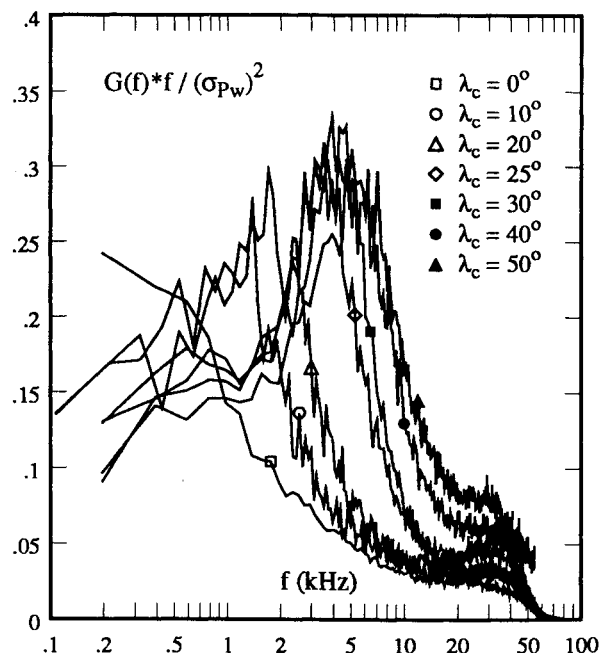

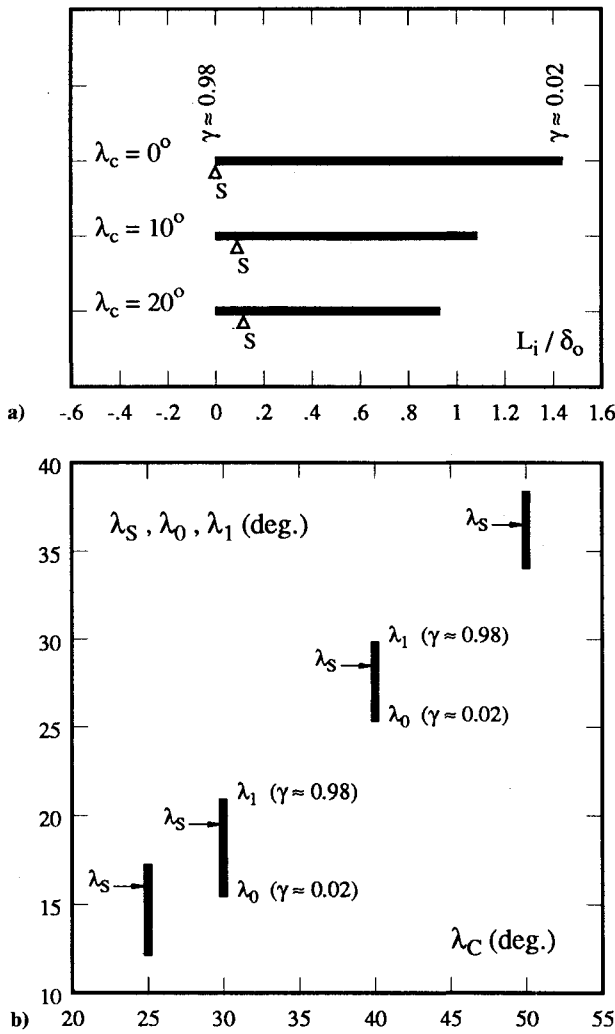**Fig. 9   Power spectral densities at $(\sigma_{Pw})_{max}$ along row O2.**

Fig. 10 Variation of intermittent region length.

Normalized power spectral densities of $X_s(t)$ in the unswept interaction, and along the outermost row of all swept interactions are plotted in Fig. 12. Each curve is identified by a marker that is described in the legend. In this representation, the area under the curve over a given range of frequencies is the contribution to the variance from that frequency range in separation shock foot position history. In other words, normalized power spectral densities show dominant frequencies in separation shock motion. Clearly, all frequencies in separation shock motion are lower than about 15 kHz. Also, dominant frequencies in separation shock motion increase as the interaction is progressively swept back. It should be noted that the same trends were observed along other rows of all swept interactions.

PDFs of $V_s(t)$ have also been calculated for upstream and downstream motions of the separation shock foot. Typical PDFs of velocity for upstream and downstream motions are plotted in Figs. 13a and 13b, respectively. Again, the probability is given by $N_i/(N_T^*W)$. Clearly, separation shock velocities are highly skewed. Mean shock velocities measured along the outermost rows in each interaction are tabulated in Table 3 for upstream $(\bar{V}_s)_u$ and downstream $(\bar{V}_s)_u$ motions of the separation shock. It appears that mean shock velocities in either direction are not measurably different. Furthermore, mean shock velocities in each interaction seem to be fairly constant and equal to about 3% of the freestream velocity. It appears that there is a slight increase in the mean shock velocities with

Dolling et al.[17] In brief, the line of coalescence in surface flow patterns, i.e., the separation line, occurs at a location where the time-averaged wall shear stress is zero. In the unswept interaction the wall shear stress in the downstream direction $(\tau_w)_d$ is much greater than the wall shear stress in the upstream direction $(\tau_w)_u$, such that the coalescence of surface streaklines occurs at the downstream end of the intermittent region. Whereas in the swept interactions, the upstream component of the wall shear stress increases appreciably, hence changing the relative position in the intermittent region where the time-averaged wall shear stress becomes zero. As a result, the line of coalescence of surface streaklines shifts progressively upstream in the intermittent region.
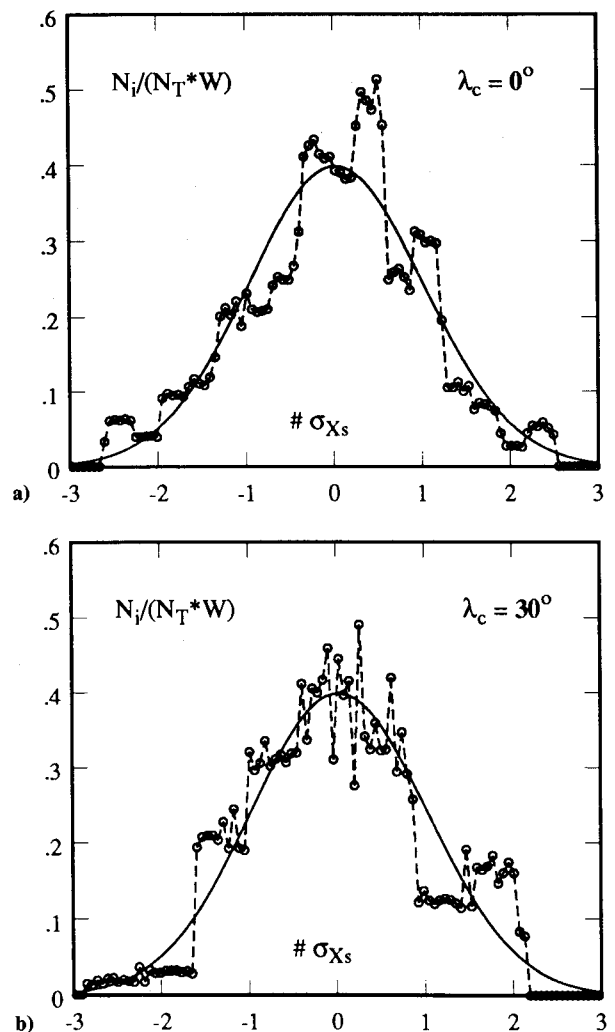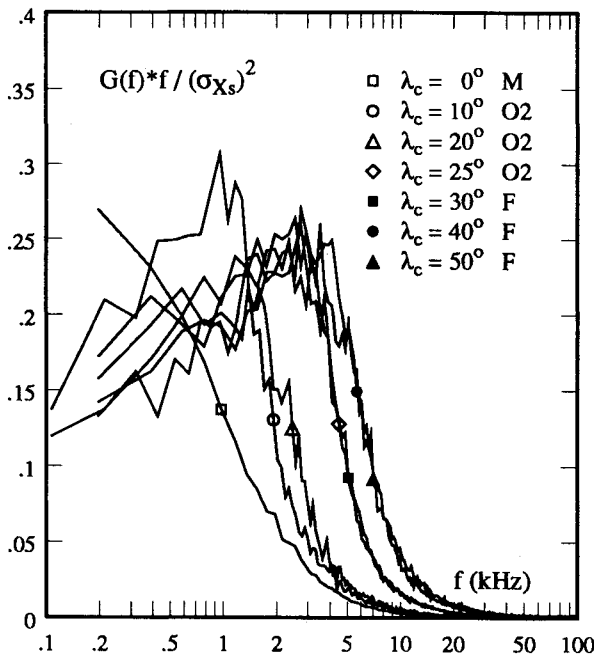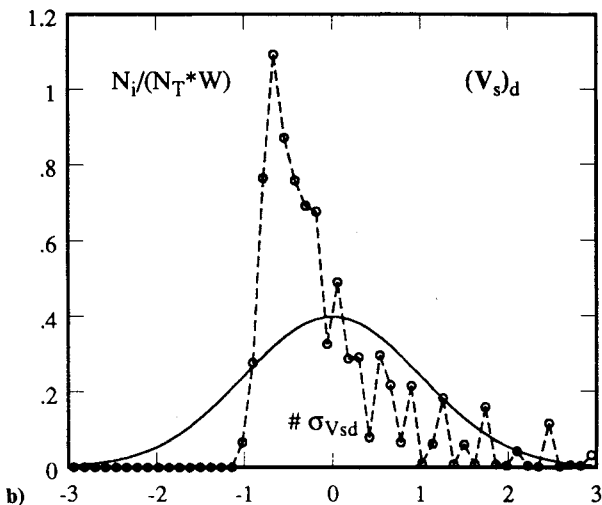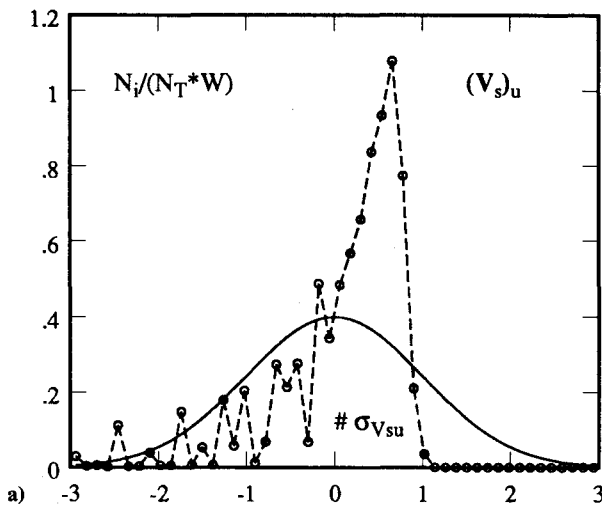
Separation Shock Dynamics

Standard time-series analysis techniques have been used to examine the separation shock foot position history $X_s(t)$ and separation shock foot velocity history $V_s(t)$, the derivations of which were explained in the Analysis Techniques section.

Figures 11a and 11b show the PDFs of the separation shock foot position along row M of the unswept and along row F of the 30-deg swept interaction, respectively. The probability is given by $N_i/(N_T^*W)$, where N_i is the number of points in bin i, N_T the total number of points, and W the width of the window. Results are plotted together with the Gaussian distribution (indicated by the solid line). Clearly, the separation shock foot is normally distributed in the intermittent region, independent of the interaction in which it is generated. It should be noted that similar results were obtained along all rows in all the interactions studied.

Fig. 11 Probability density functions of $X_s(t)$ for a) $\lambda_C = 0$ deg and b) $\lambda_C = 30$ deg.

Fig. 12 Power spectral densities of $X_s(t)$.

increasing sweep. It should be noted that mean velocities from $V_s(t)$ are calculated from all of the data as the shock moves throughout the entire intermittent region. This is advantageous in comparing separation shock velocities in different interactions since the entire motion of the separation shock is given by a single value.

To summarize, the results from conditional sampling algorithms have shown that the separation shock dynamics defined in terms of the separation shock foot history and its statistics are essentially the same in all interactions, regardless of the sweepback. The separation shock foot position in the intermittent region is normally distributed, and its velocity in either direction does not change with increasing sweep. The primary effect of sweepback on the separation shock dynamics is the decreasing of the length of its intermittent region in which the separation shock travels. Although the dominant separation shock frequencies increase with increasing sweepback, this can be attributed directly to the decrease in the length of the intermittent region.
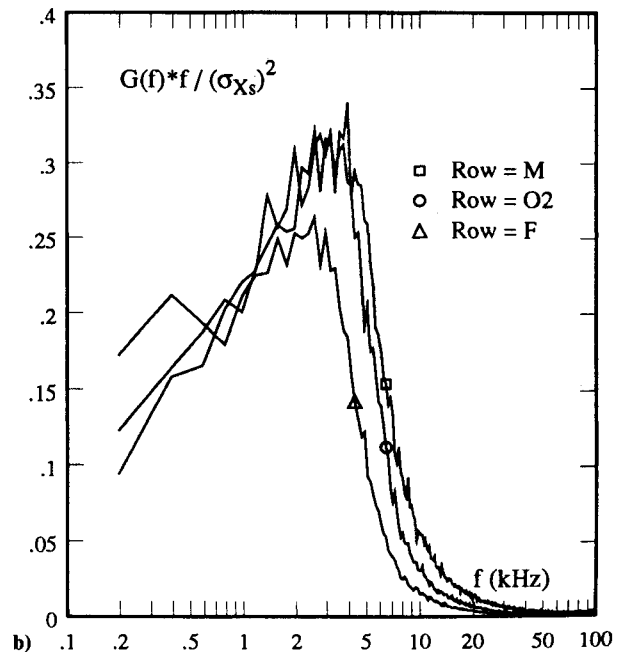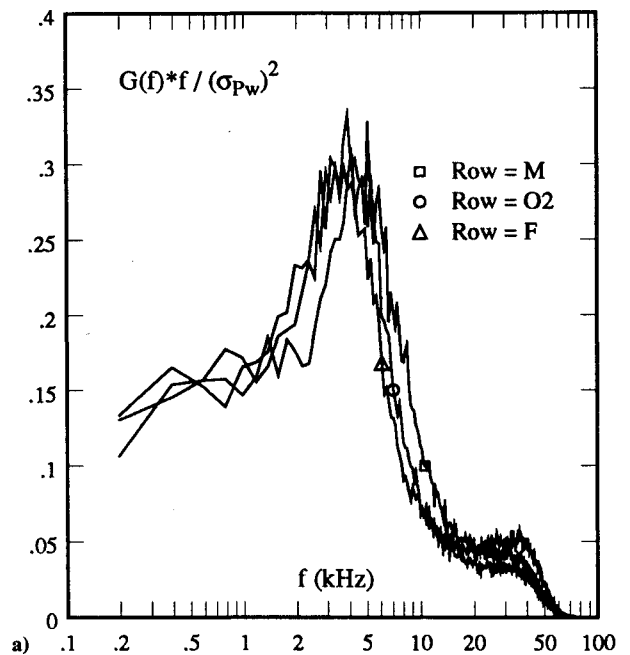

Fig. 13 Probability density functions of $V_s(t)$ for a) upstream and b) downstream velocities.

Fig. 14 Power spectral densities of a) $\bar{P}_w(t)$, and b) $X_s(t)$ for $\lambda_C = 30$ deg.

Table 3   Mean shock velocities

λ_C, deg	Row	$(\bar{V}_s)_u$, m/s (ft/s)	$(\bar{V}_s)_d$, m/s (ft/s)
0	M	−21.5 (−70.7)	22.0 (72.2)
10	O2	−20.8 (−68.1)	21.4 (70.1)
20	O2	−21.8 (−71.4)	20.8 (68.4)
25	O2	−24.4 (−79.9)	24.2 (79.3)
30	F	−26.5 (−87.1)	27.2 (89.3)
40	F	−26.1 (−85.5)	26.6 (87.4)
50	F	−23.8 (−78.2)	24.0 (78.9)

Spanwise Variations in Separation Shock Dynamics

To determine spanwise variations in the separation shock dynamics, measurements along rows M, O2, and F in the 30-deg interaction were analyzed and compared. Normalized power spectral densities of $P_w(t)$ and $X_s(t)$ measured along rows M, O2, and F in the 30-deg interaction are plotted in Figs. 14a and 14b. Each curve is identified by a marker that is described in the legend. The same trends are apparent in both figures. The dominant frequencies of the separation shock motion decrease in the spanwise direction in a given interaction. Given that all three of these rows are in the region of quasiconical symmetry and that shock velocities along each of these rows are roughly constant and equal, the only possible explanation for the decrease in the dominant frequencies of the separation shock motion is the increase in the intermittent region length scale.

Conclusions

To examine the effects of sweepback on the unsteady separation in Mach 5 compression ramp interactions, measurements of wall pressure fluctuations have been made upstream of the corner line in interactions generated by unswept and 10-, 20-, 25-, 30-, 40-, and 50-deg swept compression ramp models. The streamwise ramp angle was 28 deg in all cases. The data were analyzed using standard time-series analysis techniques and conditional sampling algorithms. The following conclusions were drawn:

1) The 10-deg interaction is cylindrically symmetric, whereas the entire span of the 20-deg interaction is within the inception zone. All highly swept interactions (i.e., $\lambda_C \geq 25$ deg) are quasiconically symmetric.

2) In highly swept interactions, the rms distributions of pressure fluctuations as well as the mean pressure distributions are essentially quasiconically symmetric. The rms levels decrease globally with increasing sweep as does the maximum rms generated by the translating separation shock.

3) The length of the intermittent region, over which the separation shock foot translates, decreases with increasing sweep. In a given interaction, the length of the intermittent region grows spanwise.

4) Dominant separation shock frequencies, observed in both surface pressure fluctuations and separation shock foot histories, increase from about 0.3–0.5 kHz for unswept flow to about 2–7 kHz in highly swept flows. In a given interaction, shock frequencies decrease spanwise.

5) Separation shock dynamics defined in terms of the shock-foot history and its statistics are essentially the same in all interactions. The separation shock foot position is normally distributed, and the mean shock velocities are essentially equal. The only difference is in the length of the region in which the separation shock moves. Higher frequencies are a direct result of the decrease in the length scale of the separation shock motion.

References

[1]Bogdonoff, S. M., "Some Experimental Studies of the Separation of Supersonic Turbulent Boundary Layers," Aeronautical Engineering Dept. Rept. 336, Princeton Univ., Princeton, NJ, June 1955.

[2]Dolling, D. S., and Murphy, M. T., "Unsteadiness of the Separation Shock Wave Structure in a Supersonic Compression Ramp Flowfield," AIAA Journal, Vol. 21, No. 12, 1983, pp. 1628-1634.

[3]Dolling, D. S., and Or, C. T., "Unsteadiness of the Shock Wave Structure in Attached and Separated Compression Ramp Flowfields," Experiments in Fluids, Vol. 3, 1985, pp. 24-32.

[4]McClure, W. B., and Dolling, D. S., "Exploratory Study of Effects of Suction near Reattachment on the Unsteadiness of a Mach 5 Compression Ramp Interaction," AIAA Paper 91-1767, June 1991.

[5]Dolling, D. S., and Brusniak, L., "Correlation of Separation Shock Motion in a Cylinder-Induced Interaction with Pressure Fluctuations under the Separated Region," AIAA Paper 91-0650, Jan. 1991.

[6]Dolling, D. S., and Brusniak, L., "Separation Shock Motion in Fin, Cylinder, and Compression Ramp-Induced Turbulent Interactions," AIAA Journal, Vol, 27, No. 6, 1989, pp. 734-742.

[7]Gramann, R. A., and Dolling, D. S., "Dynamics of Separation and Reattachment in a Mach 5 Unswept Compression Ramp Flow," AIAA Paper 90-0380, Jan. 1990.

[8]Erengil, M. E., and Dolling, D. S., "Unsteady Wave Structure near Separation in a Mach 5 Compression Ramp Interaction," AIAA Journal, Vol. 29, No. 5, 1991, pp. 728-735.

[9]Marshall, T. A., and Dolling, D. S., "Spanwise Properties of the Unsteady Separation Shock in a Mach 5 Unswept Compression Ramp Interaction," AIAA Paper 90-0377, Jan. 1990.

[10]Kussoy, M. I., Brown, J. D., Brown, J. L., Lockman, W.K., and Hortsman, C. C., "Fluctuations and Massive Separation in Three-Dimensional Shock-Wave/Boundary-Layer Interactions," 2nd International Symposium on Transport Phenomena in Turbulent Flows, Univ. of Tokyo, Tokyo, Japan, Oct. 1987.

[11]Settles, G. S., and Dolling, D. S., "Swept Shock/Boundary-Layer Interactions—Tutorial and Update," AIAA Paper 90-0375, Jan. 1990.

[12]Settles, G. S., and Dolling, D. S., "Swept Shock Wave Boundary Layer Interactions," Tactical Missile Aerodynamics, edited by M. Hemsch and J. Nielsen, Vol. 104, Progress in Astronautics and Aeronautics, AIAA, New York, 1986, pp. 297-379.

[13]Tran, T. T., "An Experimental Investigation of Unsteadiness in Swept Shock Wave/Turbulent Boundary Layer Interactions," Ph.D. Dissertation, Mechanical and Aerospace Engineering Dept., Princeton Univ., Princeton, NJ, March 1987.

[14]Tan, D. K. M., Tran, T. T., and Bogdonoff, S. M., "Surface Pressure Fluctuations in a Three Dimensional Shock Wave Turbulent Boundary Layer Interaction," AIAA Paper 85-0125, Jan. 1985.

[15]Tran, T. T., Tan, D. K. M., and Bogdonoff, S. M., "Surface Pressure Fluctuations in a Three Dimensional Shock Wave Turbulent Boundary Layer Interaction at Various Shock Strengths," AIAA Paper 85-1562, July 1985.

[16]Schmisseur, J. D., and Dolling, D. S., "Unsteady Separation in Sharp Fin-Induced Shock Wave/Turbulent Boundary Layer Interaction at Mach 5," AIAA Paper 92-0748, Jan. 1992.

[17]Dolling, D. S., Boitnott, T., and Erengil, M. E., "Effects of Moderate Sweepback on the Separation Shock Wave Dynamics in a Mach 5 Compression Ramp Interaction," AIAA Paper 91-0254, Jan. 1991.

[18]McClure, W. B., private communication, Oct. 1991.

[19]Boitnott, T., "An Experimental Study of the Dynamics of Moderately Swept Compression Ramp-Induced Separation at Mach 5," M.S. Thesis, Dept. of Aeronautical Engineering and Engineering Mechanics, Univ. of Texas, Austin, TX, Aug. 1990.

[20]Settles, G. S., and Kimmel, R. L., "Similarity of Quasi-Conical Shock Wave Turbulent Boundary Layer Interactions," AIAA Journal, Vol. 24, No. 1, 1986, pp. 47-53.